International Journal of Biological Macromolecules 227 (2023) 805–814

Contents lists available at ScienceDirect

International Journal of Biological Macromolecules

journal homepage: www.elsevier.com/locate/ijbiomac

Synthesis of luminescent chitosan-based carbon dots for *Candida albicans* bioimaging

Bruno Peixoto de Oliveira [a,c,*], Nathalia Uchoa de Castro Bessa [b], Joice Farias do Nascimento [a], Carolina Sidrim de Paula Cavalcante [a], Raquel Oliveira dos Santos Fontenelle [a], Flávia Oliveira Monteiro da Silva Abreu [a]

[a] Program in Natural Sciences, State University of Ceará (UECE), Fortaleza 60.714-903, CE, Brazil
[b] Natural Polymers Laboratory, Department of Chemistry, State University of Ceará (UECE), Fortaleza, CE, 60.714-903, Brazil
[c] Educators Training Institute, Federal University of Cariri (UFCA), Brejo Santo, CE, 63.260-000, Brazil

ARTICLE INFO

Keywords:
Carbon dots
Chitosan
Factorial design
Quantum yield
Bioimaging agent

ABSTRACT

In this work, we used chitosan as a raw material to synthesize carbon dots using fast microwave carbonization. We studied the influence of the synthesis time, doping agent, and the molar ratio between the reactants on the quantum yield of carbon dots. Chitosan-based carbon dots displayed stable blue fluorescence emission with excitation-dependent behavior and quantum yield values ranging from 1.16 to 7.07 %. ANOVA results showed that the interaction factor between the doping agent and the molar ratio of the reactants was a significant combination to produce carbon dots with higher quantum yield. The presence of the doping agent improved the carbon dots optical properties by obtaining higher fluorescence intensity values. Confocal laser microscope images showed that the carbon dots internalized in the *Candida albicans* cellular membrane, exhibiting blue, green, and red emissions, acting as a promising agent for bioimaging.

1. Introduction

Carbon dots (CDs) are the newest fluorescent carbon nanomaterials member [1]. CDs have attracted researchers' attention because of their properties, such as high solubility and stability, biocompatibility, and low toxicity [2]. The applications in many fields, such as sensors, photocatalysis, drug delivery systems, and solar cell make them of great economic and technological value [3–5].

Several synthesis methods, such as hydrothermal, arc discharge, laser ablation, and carbonization are usually applied to produce CDs [6]. They are grouped into two approaches: top-down and bottom-up. Microwave pyrolysis, one of the bottom-up approaches, is an environmentally friendly, cost-effective, and well-established method for CDs synthesis [7,8]. In contrast with other heating methods, this approach heats directly the target molecule, resulting in faster reaction times [9]. Also, uniform heating provided by microwaves could form particles with a uniform size distribution [10,11].

Different raw materials for microwave CDs synthesis may be used, such as eggshell membranes, citric acid, and glucose [12–14]. Because of its constitution with a high amount of hydroxyl (-OH) and amino ($-NH_2$) functional groups, chitosan is a suitable raw material for CDs synthesis [15]. Chitosan is a natural linear polycationic polysaccharide comprising β-(1,4)- linked 2-amino-2deoxy-D-glucose residues, the second most abundant natural polymer, and exhibits several physical properties such as viscosity, mucoadhesivity, and possible solubility in various media [16–18].

Applications of chitosan-based CDs in ion sensing, cell imaging, and drug delivery demonstrate the material's versatility [19–22]. Also, compared with traditional bioimaging agents, like organic dyes, quantum dots, and upconversion nanoparticles, previous research has established that CDs possess the desirable characteristics for use as a bioimaging agent, namely bright, non-toxic, and biocompatible materials, and are stable against photobleaching [23,24]. However, to the best of our knowledge, there is no existing report on the use of chitosan-based CDs for *Candida albicans* bioimaging.

The origin of the CDs fluorescence is still under debate, where the intensity and the quenching mechanisms depend on the starting material and the doping agent [25,26]. However, research to date has not yet determined the influence of synthesis factors on the CDs' quantum yield, which is desirable to amplify bioimaging applications of CDs.

* Corresponding author at: Graduate Program Sciences, State University of Ceará (UECE), Fortaleza, 60.714-903, CE, Brazil.
E-mail address: bruno.peixoto@aluno.uece.br (B.P. Oliveira).

https://doi.org/10.1016/j.ijbiomac.2022.12.202
Received 14 September 2022; Received in revised form 14 December 2022; Accepted 17 December 2022
Available online 20 December 2022

Table 1
Quantum yields measurements obtained in different synthesis conditions.

#	Sample	Independent variables			Dependent variable	
		Doping agent A[a]	Synthesis time [min] B[b]	Molar ratio [mol/mol] C[c]	Quantum yield [%]	Fluorescence intensity [a.u]
1	CDQ5S9	−1	−1	−1	4.01 ± 1.17	5110.4
2	CDQ5D9	+1	−1	−1	3.19 ± 0.29	28,343.7
3	CDQ5S15	−1	+1	−1	2.98 ± 0.06	6289.1
4	CDQ5D15	+1	+1	−1	6.17 ± 2.87	16,471.8
5	CDQ22S9	−1	−1	+1	7.07 ± 0.32	110,681.1
6	CDQ22D9	+1	−1	+1	4.46 ± 0.59	42,040.7
7	CDQ22S15	−1	+1	+1	1.16 ± 0.33	99,357.6
8	CDQ22D15	+1	+1	+1	4.40 ± 0.11	43,174.9

[a] (Factor A: Doping Agent. High level (+) = doping agent presence; low level (−) = doping agent absence).
[b] (Factor B: Synthesis time. High level (+) = 15 min; low level (−) = 9.5 min)
[c] (Factor C: Reactants' molar ratio (n_{ac}:n_{chit}). High level (+) = 22:1; low level (−) = 6:1).

In this work, we evaluated the effect of synthesis parameters on the quantum yield and fluorescence intensity of chitosan-based carbon dots synthesized using a simple microwave method. We performed structural and optical analysis to understand the influence of parameters on the CDs' properties. Moreover, the chitosan-based carbon dots were applied as a bioimaging agent for *Candida albicans*. In our findings, CDs exhibited excellent fluorescent properties and exhibit high affinity to fungal cellules, and successfully serve as effective fluorescent markers of biological cells.

2. Materials and methods

2.1. Materials

Chitosan (Degree of deacetylation = 90.0 %, MW = 21,4 KDa, Êxodo, Brazil), glacial acetic acid (Neon, Brazil), and 1,2-ethylenediamine (Neon, Brazil) were the reactants. The reactants had analytical grade and were used without any further treatment.

2.2. Factorial design and CDs synthesis

We developed a 2^3 factorial design to investigate the synthesis parameters' influence on the quantum yield and fluorescence intensity of chitosan-based CDs synthesized by microwave. The independent variables were doping agent (A), synthesis time (B), and the molar ratio of acetic acid/chitosan (C), which were measured at two levels (Table 1).

- Factor A: Doping Agent. High level (+) = doping agent presence; low level (−) = doping agent absence.
- Factor B: Synthesis time. High level (+) = 15 min; low level (−) = 9.5 min).
- Factor C: Reactants' molar ratio (n_{ac}:n_{chit}). High level (+) = 22:1; low level (−) = 5:1).

The CDs synthesis was adapted from the report of Gong et al. [27]. Briefly, it was dissolved by stirring a specific amount of chitosan (0.5 or 1.0 g) and 5 ml of doping agent (ethylenediamine) in 10 ml of the glacial acetic acid solution (1 or 8 %). After the dissolution, the product was placed in a domestic microwave at 700 W (Philco-PMO33B) and submitted to thermal treatment for a predetermined time. After treatment, all samples were redispersed in 20 ml of distilled water and centrifuged at 4000 rpm for 30 min. The supernatant was collected, filtered, and dialyzed (Spectra/Por®6 dialysis membrane − 1 kDa MWCO) against distilled water for three days to remove impurities.

2.3. Characterization and data analysis

The morphology of CDs was investigated by atomic force microscopy (Shimadzu SPM-9700). Samples were fixed on a glass coverslip. The analysis was performed in intermittent contact mode, constant force of 42 N/m, frequency of 320 kHz, and scan rate of 1 Hz.

The CDs main functional groups were analyzed by Fourier transform infrared spectroscopy (FTIR) in a Nicolet iS5 (Thermo Scientific). The samples were analyzed using an attenuated total reflection sensor in a spectrometer. The scanning was performed in the wavelength range of 400 cm^{-1} to 4000 cm^{-1}, with a resolution of 4 cm^{-1}. For the analysis of Zeta potential, 1 ml of the previously stirred dispersions was diluted in 100 ml of deionized water, homogenized, and subjected to analysis in the Zetasizer NanoZS equipment (Malvern). The readings were performed in triplicate.

The elemental analysis of C, H, and N was performed in the CHNS/O Analyzer 2400 Series II equipment (Perkin Elmer). The samples were weighed adopting a range between 1 and 2 mg in tin capsules for solids, specific for elemental analysis. In the case of liquid samples, we used liquid containers with the same specificity. In both cases, we used an ultra-precision micro scale to measure the masses. The temperatures of the combustion and reduction columns were 950 °C and 640 °C, respectively. The gas pressures O_2 and He were 140 KPa and 105 KPa, respectively. The filling time of the combustion column was 30s. The total analysis time was approximately 5 min.

The absorption and fluorescence spectra of the CDs were recorded respectively in the spectrophotometer UV–VIS (Shimadzu UV-2600) and spectrofluorophotometer (Shimadzu RF-6000). The absorption spectra was performed to elucidate the wavelengths at which absorptions of carbon dots occur. The fluorescence spectra varied to observe the maximum fluorescence intensity of chitosan-based carbon dots [28].

The variance analysis (ANOVA), with 95 % reliability was performed in Microsoft Excel® software to evaluate the influence of parameters on the fluorescence intensity and quantum yield of CDs synthesized by microwave.

2.4. Quantum yield (QY) determination

In the CDs quantum yield measurements, the absorbance of samples was kept below 0,05 to avoid inner filter effects [29]. The QY was determined using Eq. 1:

$$QY = QY_{ref} \times \frac{I}{I_{ref}} \times \frac{A_{ref}}{A} \times \frac{n^2}{n_{ref}^2} \quad (1)$$

QY is the quantum yield of CDs; I is the integrated emission intensity; A is the absorbance measured at 350 nm; and n is the refractive index. The ref. subscript is related to the quinine sulfate.

2.5. Cellular viability assay

The cellular viability was quantified by the ability of living cells to reduce the yellow dye 3-(4,5-dimethyl-2-thiozolyl)-2,5-diphenyl-2H-tetrazolium bromide (MTT) to a purple formazan product [30]. For the experiments, cells were plated in 96-well plates (0.7×10^5 cells/ml). After 24 h, chitosan-based carbon dots was added to each well and the

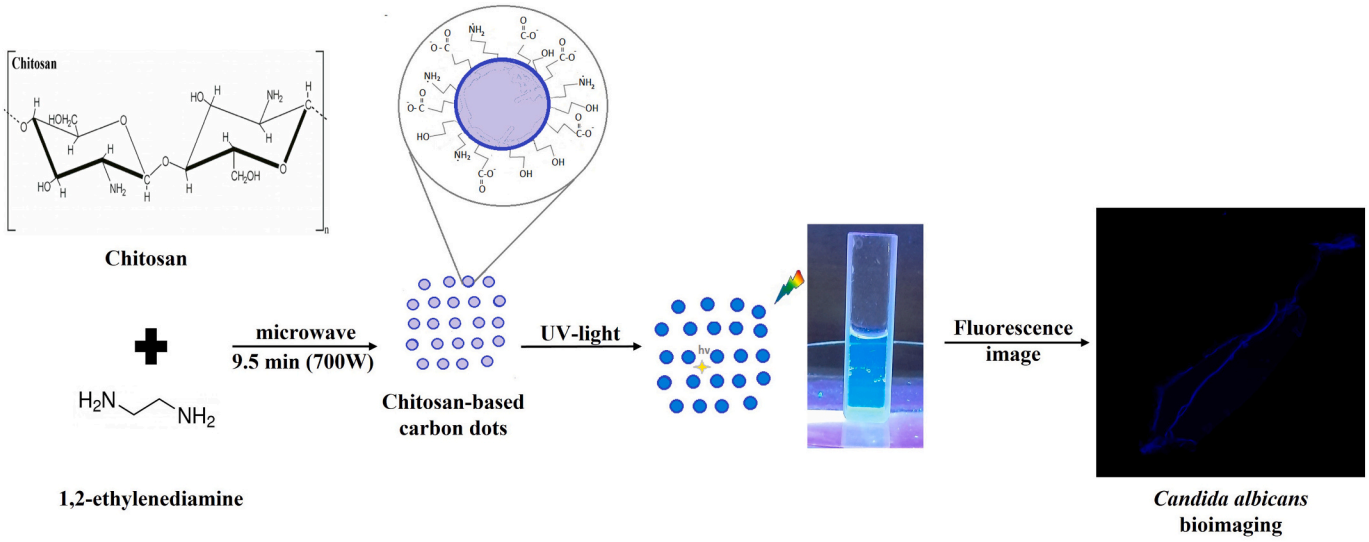

Fig. 1. Schematic representation of chitosan-based CDs synthesis and application for *Candida albicans* cells' bioimaging.

cells incubated for 24 h. Thereafter, the plates were centrifuged, and the medium was replaced by fresh medium (150 μl) containing 0.5 mg/ml MTT. Three hours later, the MTT formazan product was dissolved in 150 μl DMSO, and the absorbance was measured using a multiplate reader (Spectra Count, Packard, Ontario, Canada). Drug effect was quantified as the percentage of control absorbance of the reduced dye at 595 nm. Methyl methanesulfonate (MMS) at 4×10^{-5} M was used as positive control.

2.6. Fluorescence imaging of Candida albicans

The standard *C. albicans* strain was obtained from the American Type Culture Collection (ATCC 90028). The inoculum was prepared from *C. albicans* cells cultured on Sabouraud Dextrose Agar (SDA) and incubated at 35 °C for 24 h. Yeast colonies were transferred to tubes containing sterile PBS to obtain suspensions with a turbidity equivalent to 0.5 on the McFarland scale (10^6 CFU ml^{-1}). These suspensions were then diluted at 1:2000 with an RPMI 1640 medium, supplemented with L-glutamine, and incubated with chitosan-based CDs (10 μg/ ml) for 1 h. The fluorescence images were captured by a confocal laser microscope (LM-710, Carl Zeiss) in three excitation levels, namely 405, 488, and 561 nm.

3. Results and discussion

The suspensions of synthesized CDs presented distinct colors, ranging from light yellow and deep brown, showing sundry carbonization degrees, according to Wang et al. [31]. Samples displayed blue fluorescence under UV light at 360 nm. Fig. 1 shows the schematic representation of CDs synthesis, properties, and application for bioimaging. The potential mechanism for CDs formation from chitosan is described by Marinovic, which requires the hydrolysis of chitosan precursor to glucosamine, then dehydration, polymerization, and condensation steps [32].

The degree of deacetylation is an important characteristic of chitosan since it is proportional to the number of free amino groups, which can be protonated in acid medium (NH_3^+) [33]. Also, the number of free amino groups is significant in the properties of chitosan [34]. The functional groups shown in the structure of the carbon dots are linked to the starting material. The higher degree of deacetylation of chitosan (90 %) provides more amino groups available in the chitosan matrix. The amino groups, through covalent bonds, will be more easily incorporated into the core of the carbon dots, increasing the degree of functionalization and their quantum yield [35].

3.1. Fluorescence intensity and quantum yield variance analyses

Table 2 indicates ANOVA results of the effects on the CDs fluorescence intensity. We observe by the superior median square (MQ) and the F_0 values that the main factor in the fluorescence intensity of CDs is the molar ratio between chitosan and acetic acid (factor C). In addition, there was an interaction effect between doping agent and molar ratio (Interaction AC). The synthesis time did not indicate significant variation in the fluorescence intensity of the CDs. The different fluorescence intensities were due to modifications in the chemical structure of carbon dots.

The doped sample has higher nitrogen content, consequently more surface states capable of increasing the fluorescence intensity of the CDs. [36,37]. The most widely accepted luminescence mechanism is the CD's surface states. Also, different surface functional groups can introduce diverse fluorophore groups or energy levels in CDs [37].

We verified the effect of molar ratio acid:chitosan (factor C) through

Table 2
ANOVA analysis of the influence of synthesis parameters in the fluorescence intensity of chitosan-based carbon dots.

Variance analysis									
A	B	C	AB	AC	BC	ABC	Sqerror	SQ_{total}	
−91.41	−20.88	239.04	−0.59	−158.24	0.50	25.51			Contrast
−22.85	−5.22	59.76	−0.15	−39.56	0.13	6.38			Effect
1044.41	54.51	7142.47	0.04	3129.95	0.03	81.33	135.92	11,452.75	SQ
1.00	1.00	1.00	1.00	1.00	1.00	1.00	8.00		GL
1044.41	54.51	7142.47	0.04	3129.95	0.03	81.33	16.99		MQ
7.68	0.401	52.549	0.0003	23.02	0.0002	0.598			F_0
11.259	11.259	11.259	11.259	11.259	11.259	11.259			$F_{critical}$

Table 3
ANOVA analysis of the influence of synthesis parameters in the quantum yield of chitosan-based CDs.

Variance analysis									
A	B	C	AB	AC	BC	ABC	Sqerror	SQ_{total}	
18.00	−24.20	4.52	59.12	−10.52	−47.40	−11.16			Contrast
0.75	−1.01	0.19	2.46	−0.44	−1.98	0.47			Effect
6.75	12.20	0.43	72.82	2.31	46.81	2.59	51.00	194.97	SQ
1.00	1.00	1.00	1.00	1.00	1.00	1.00	41.00	48,00	GL
6.75	12.20	0.43	72.82	2.31	46.81	2.59	1243		MQ
5.43	9.81	0.34	58.57	1.85	37.65	2.09			F_0
7.30	7.30	7.30	7.30	7.30	7.30	7.30			$F_{critical}$

the fluorescence intensity average values. At the 22:1 molar ratio, the higher concentration of acetic acid caused protonation of the amino groups present in the chitosan structure [33]. N-containing functional groups will make CDs positively charged and obtained different passivation degree [38]. There may have been a greater degree of functionalization of the carbon dots with a greater number of amino groups on their surface. Also, N-surface states facilitate a high yield of radiative recombination improving their fluorescence [39].

In the higher molar ratio (22:1 acid:chitosan), the fluorescence intensity achieved higher average values (73,814 a.u) than in the lower molar ratio (14,054 a.u). The higher fluorescence intensity obtained can be explained by the higher number of surface states generated by the functionalization of the carbon dots. By tunning the surface structure of CDs through functionalization, it is possible to change the electronic energy level and modulate the optical behavior [40]. In effect, the fluorescence intensity was improved, and this effect is desirable for bioimaging applications.

We also observed a synergistic effect between the doping agent and the molar ratio (factor AC) on the fluorescence intensity. In our study, ethylenediamine as a doping agent significantly increased the fluorescence intensity (28,344 and 16,472 a.u) in contrast to the non-doped sample (5110 and 6289 a.u). However, this effect was observed only at the lower acid: chitosan molar ratio. According to the literature, introducing nitrogen groups changes the CDs' composition, diminishing the oxygen content and increasing the CDs nitrogen content, corroborating our results [13]. Moreover, the synthesis parameters and nature of doping agents are crucial for dictating the CDs optical properties.

In higher acid:chitosan molar ratio, we observed an inversion in the results of the fluorescence intensities. The presence of the doping agent decreased the fluorescence intensity, assuming values of 42,041, 43,175 a.u and 110,681, 99,358 a.u for doped and non-doped samples, respectively. Here, the acid excess in the medium may function as a direct reactant with the ethylenediamine, a Lewis base, to produce an organic salt, which is an undesirable side product. This scenario partially prevented the insertion of the doping agent into the CD's structure. Lima et al. related results with higher reactant levels and acetylation agents that could generate side products [41].

Table 3 indicates ANOVA results of the effects on the CDs quantum yield. We observe by the superior median square (MQ) and the F_0 values ($F_0 > F_{critical}$) that the main effects on the quantum yield is the synthesis time (factor B), the interaction effect between the doping agent and synthesis time (factor AB), and the interaction effect between synthesis time and acid:chitosan molar ratio (factor BC). The main factors doping agent and molar ratio did not indicate significant variation in the CDs quantum yield, showing that there is a crucial combination between the parameters, which are more relevant than the isolated individual parameters.

The effect of factor B, the synthesis time, was verified through the quantum yield average values. There is sufficient evidence showing that carbon dots retain the properties of molecular precursors under proper pyrolysis conditions [22]. In the shorter synthesis time (9.5 min), the quantum yield achieved higher values than with the longer synthesis time (15 min), with average values of, respectively, 4.68 % and 3.67 %. The highest quantum yield (7.07 %) was achieved using a shorter synthesis time (9.5 min).

In the study performed by Gong et al., chitosan-based CDs produced by microwave presented the highest quantum yield (5.50 %) with an intermediary synthesis time of 15 min, and the molar ratio acetic acid: chitosan obtained was approximately 8:1 [42]. The synthesis time after 15 min could generate excessive sample carbonization, diminishing the quantum yield, observed in our study, and in accordance with the report of Gong *et al* [42].

However, our study advances this discussion by evaluating the three parameters (doping agent, synthesis time, and molar ratio) jointly by factorial design combined with variance analysis on the quantum yield of chitosan-based CDs.

We observe a synergistic effect between the doping agent and synthesis time (factor AB), which indicated the uppermost influence on the quantum yield ($F_0 > F_{critical}$). When the doping agent is present in the solution, the longer synthesis time produced CDs with higher quantum yield results (5.28 %). Without the addition of the doping agent, a longer synthesis time does not lead to an increase in the quantum yield; instead, a decrease in average quantum yield values is observed (2.07 %). The synergy between the doping agent and synthesis time leads to a higher quantum yield (7.07 %) in a shorter synthesis time (9.5 min). At the time of 9.5 min, the quantum yield is increased without the addition of the doping agent. However, with the addition of the doping agent, the increase in quantum yield is observed only in the longer syntheses.

Statistical analysis allowed the evaluation of the influence of the synthesis parameters on the quantum yield of the carbon dots. Our results pointed out that the combination of the absence of the doping agent and a longer synthesis time was more effective in achieving higher quantum yields compared to the effect of the doping agent alone.

Manioudakis et al. reported a positive correlation between the quantum yield and the number of carboxylic groups during the condensation reaction with amines in the CDs synthesis [13].

We observed an inverse relationship between the synergy of synthesis time and molar ratio (Factor BC). In a longer synthesis time, the highest molar ratio produced CDs with a higher average quantum yield (5.76 %). The combination of shorter synthesis time and higher molar ratio achieved the highest value (7.07 %). Probably, the higher acetic acid content caused more protonation of the amino groups of chitosan and generated more surface states, even in the shorter synthesis time [33]. Effective surface functionalization of carbon particles is a necessary condition for high fluorescence performance of carbon dots [23]. In our experiments, the highest quantum yield was obtained under the conditions of no doping agent, 9.5 min synthesis, and 22:1 chitosan acid molar ratio.

However, with a longer synthesis time, CDs with higher quantum yields were produced using lower acetic acid:chitosan molar ratio (4.57 %). In higher concentrations of carbon sources, collateral reactions could happen and inhibit the formation of CDs [43].

Pal and coworkers performed a study with variation in the molar ratio of reactants in boron and phosphorus-doped CDs [43]. The higher molar ratios of boric acid and citric acid (above 11 % *w*/w) resulted in incomplete carbonization of the starting material, consequently

Table 4
Summary of chitosan-based CDs quantum yield.

Synthesis method	Synthesis time	Doping agent	Quantum Yield	Reference
Carbonization	2 h	Absence	4.34 %	[20]
Solvothermal	12 h	1,2-Ethylenediamine	5.70 %	[43]
Microwave	9.5 min	Absence	6.40 %	[44]
Microwave	15 min	1,2-Ethylenediamine	6.80 %	[27]
Microwave	15 min	Absence	5.33 %	[42]
Microwave	9.5 min	Absence	7.07 %	This work
Microwave	15 min	1,2-Ethylenediamine	6.17 %	

decreasing the luminescent quantum yield of the nanomaterial. The excess of boron in the reaction mixture lowered the efficiency of the reaction.

The quantum yield values varied from 1.16 to 7.07 % (Table 1). Our best quantum yield results are comparable or superior to other chitosan-based CDs synthesized in other reports (Table 4). Liu and coworkers produced CDs by chitosan carbonization with a synthesis time of 2 h without a doping agent with a quantum yield of 4.34 % [20]. By a 12 h solvothermal synthesis, Zhang et al. achieved chitosan-based CDs with a quantum yield of 5.70 % [44]. Dong and coworkers synthesized chitosan-based CDs by microwave approach using a synthesis time of 15 min with a quantum yield of 6.80 % using 1,2-ethylenediamine as a doping agent [27]. Our approach resulted in a higher quantum yield (7.07 %) in a shorter synthesis time (9.5 min) without a doping agent.

3.2. Structural and optical properties

By one-step microwave synthesis, we synthesized doped and non-doped chitosan-based CDs, varying the synthesis time, and using different acetic acid/chitosan molar ratios. Results demonstrated a distinct pattern for doped samples and non-doped CDs. Characterization will be addressed by comparison of doped CDs with non-doped ones using CDQ5D15 (N-doped) and CDQ22S9 (undoped) samples due to their higher quantum yields.

The CDs, after dialysis, are uniform and spheroidal with an average diameter of 15 nm for N-doped CDs and 9.7 nm for non-doped CDs. Fig. 2 shows the AFM images with self-assembling structures of nanomaterial. The size of synthesized chitosan-based CDs is comparable to other reports in the literature [45–47].

We investigated the surface charge of chitosan-CDs by Zeta potential measurement (Fig. 3). In the non-doped sample, the zeta potential was

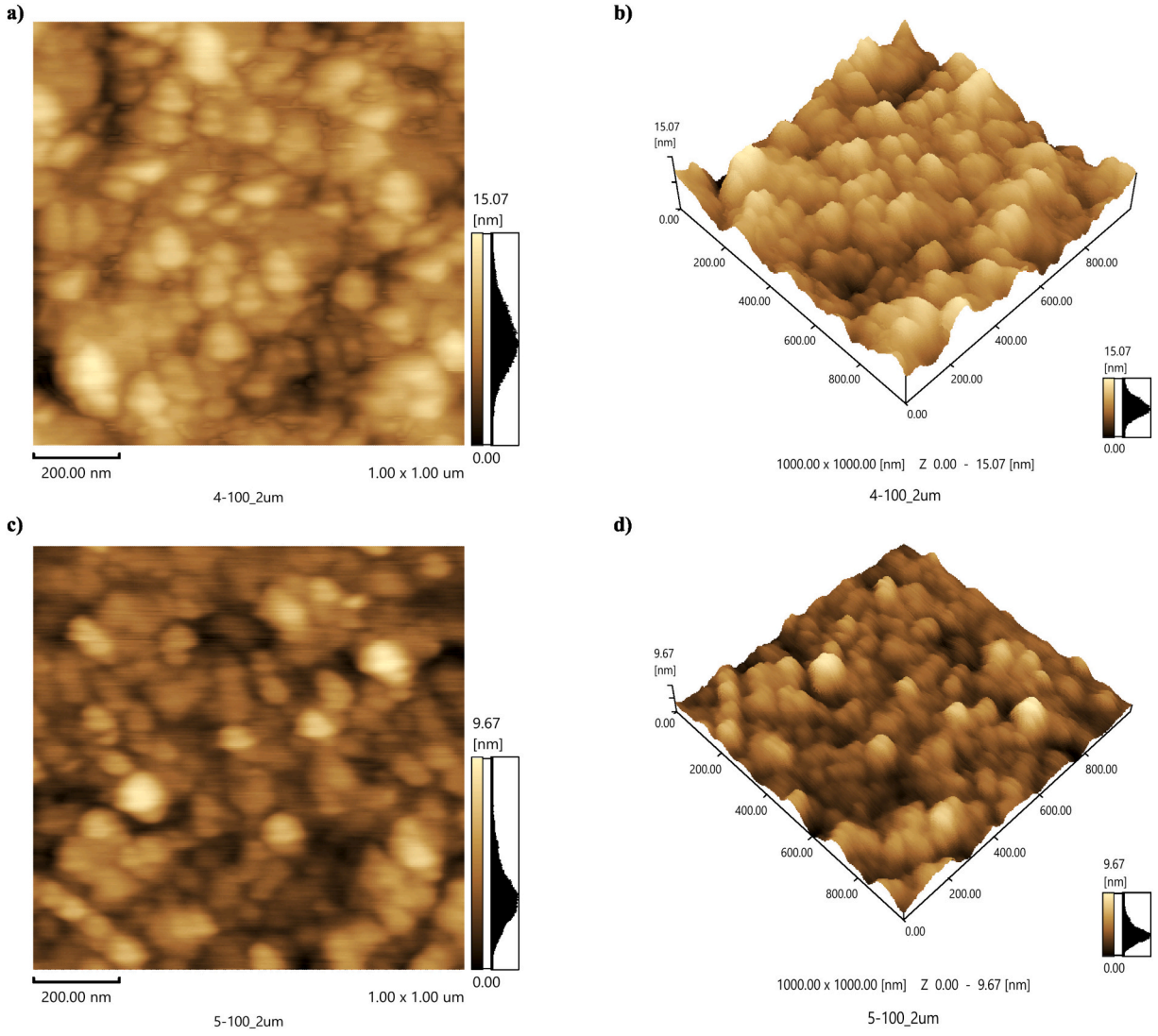

Fig. 2. (a) Topographic and 3D (b) atomic force microscope images of doped chitosan CDs with ethylenediamine with a synthesis time of 15 min (CDQ5D15); (c) Topographic and 3D (d) image of chitosan CDs without dopant with a synthesis time of 9 min (CDQ22S9).

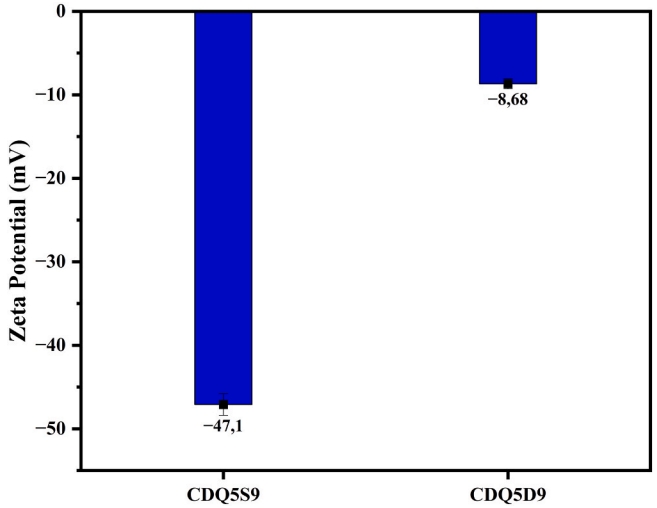

Fig. 3. Zeta potential of CDQ5S9 and CDQ5D9 samples.

Table 5
Properties of doped and non-doped chitosan CDs.

	Sample	Size (nm)	Zeta potential (mV)	Elemental composition (%)			
				C	H	N	O
1	CDQ22S9	9.7	−47.1 ± 1.3	27.01	6.78	4.27	61.94
2	CDQ5D15	15	−8.7 ± 0.6	32.22	5.36	7.43	54.99

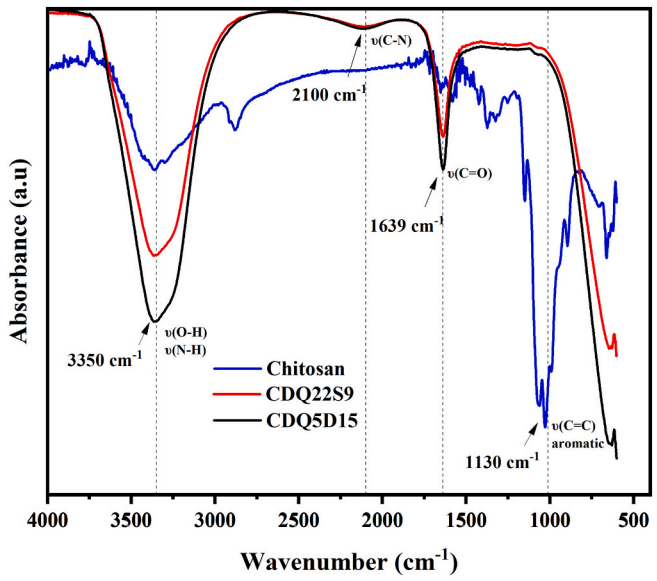

Fig. 4. FTIR spectra of non-doped, doped chitosan-based CDs and pure chitosan.

−47.1 mV, and the doped was −8.7 mV. We could attribute the different values to the ionization of oxygen-containing groups on the surface of non-doped CDs (–COOH, –OH functional groups) [48]. Doped CDs with ethylenediamine present amino groups (-NH_2), which present a positive surface charge because of the protonation in an aqueous medium.

These results confirm the pattern shown in AFM images; zeta potential values close to zero show the tendency of CDs assembly. However, the existence of a higher number of functional groups may improve the optical and fluorescence properties [49].

Elemental analysis showed that the doped and non-doped CDs have different compositions, especially regarding O/N ratio (Table 5). Non-doped and doped CDs samples have an O/N ratio of respectively 14.5 and 7.39. By comparison, the doping agent increased the nitrogen content twice in the samples. CDs with higher nitrogen content can present improvements in the optical properties of the CDs, for example, the fluorescence intensity [50].

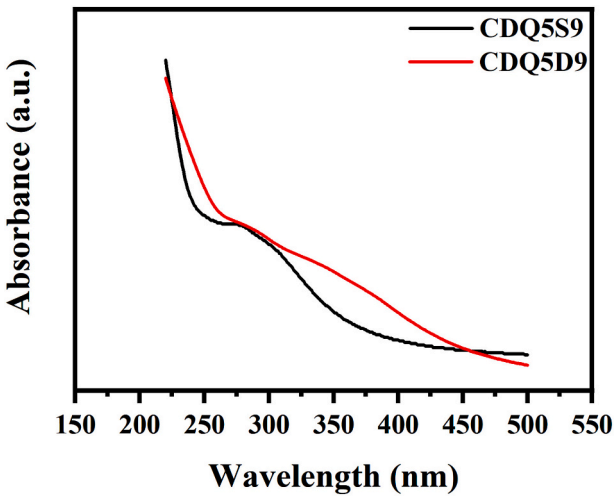

Fig. 5. UV absorption spectra of CDQ5S9 sample and CDQ5D9 sample.

FTIR spectra of chitosan-based CDs was conducted to evidence the main functional groups (Fig. 4). Doped and non-doped CDs showed depict peaks in 3350 cm^{-1} attributed to O—H and N—H stretching vibrations, 2100 cm^{-1}, 1639 cm^{-1} attributed to C—N and C═O stretching vibrations, and 601 cm^{-1} corresponding to the aromatic stretching [44,48,51–55]. The doped sample showed higher intensity in the characteristic peaks compared to the undoped sample, indicating a higher number of functional groups, which can be attributed to the successful insertion of ethylene-diamine in the CDs surface, increasing the relative nitrogen content of the CDQ5D15.

The functional groups incorporated in the CDs core improve the solubility of chitosan-based CDs [56]. Compared to the spectrum of pure chitosan, we observe the disappearance of bands in 1130 cm^{-1}, which indicates the decomposition process of pyranose rings during carbonization, which is in accordance with the study of Zhan *et al* [18]. We also noted a decrease in the absorption in the 3350 cm^{-1} and 2985 cm^{-1} bands, which is consistent with other studies [20,48].

UV-VIS absorption spectra (Fig. 5) of the non-doped sample (CDQ5S9) depict a noticeable absorption peak at 278 nm assigned to the π-π* conjugate transition of the C═C sp^2 bond in the carbon core of chitosan-based CDs. This peak is also present in the doped sample. Absorption peaks in the 200–350 nm range are characteristics of CDs [57]. Regarding the doped sample (CDQ5D9), we found a lower peak in the 320–330 nm region attributed to the formation of excited defect surface states induced by the N-doping agent [58,59].

When looking at the fluorescence spectroscopy of the samples, a clear pattern is presented, which is the excitation-dependent behavior of fluorescence properties in the non-doped CDs (Fig. 6a-b). Excitation-dependent emission is standard behavior for CDs [58,59]. On the other hand, the N-doped CDs presented the independent-excitation behavior (Fig. 6c-d). The excitation-independent behavior suggests that the fluorescence properties of CDs are related to narrow size distribution and uniform surface chemistry, in accordance with Yu et al. [60]. Nitrogen doping caused the formation of new surface states. The electrons trapped by the surface states could facilitate radiative recombination leading to the CDs emission-independent behavior [61].

In the lower acid:chitosan molar ratio (Fig. 6c), the doping agent increased the fluorescence intensity to values above 30,000 a.u. This effect of improvement of fluorescence intensity is according to other literature reports [13,50]. Barman et al. relate the gain of fluorescence

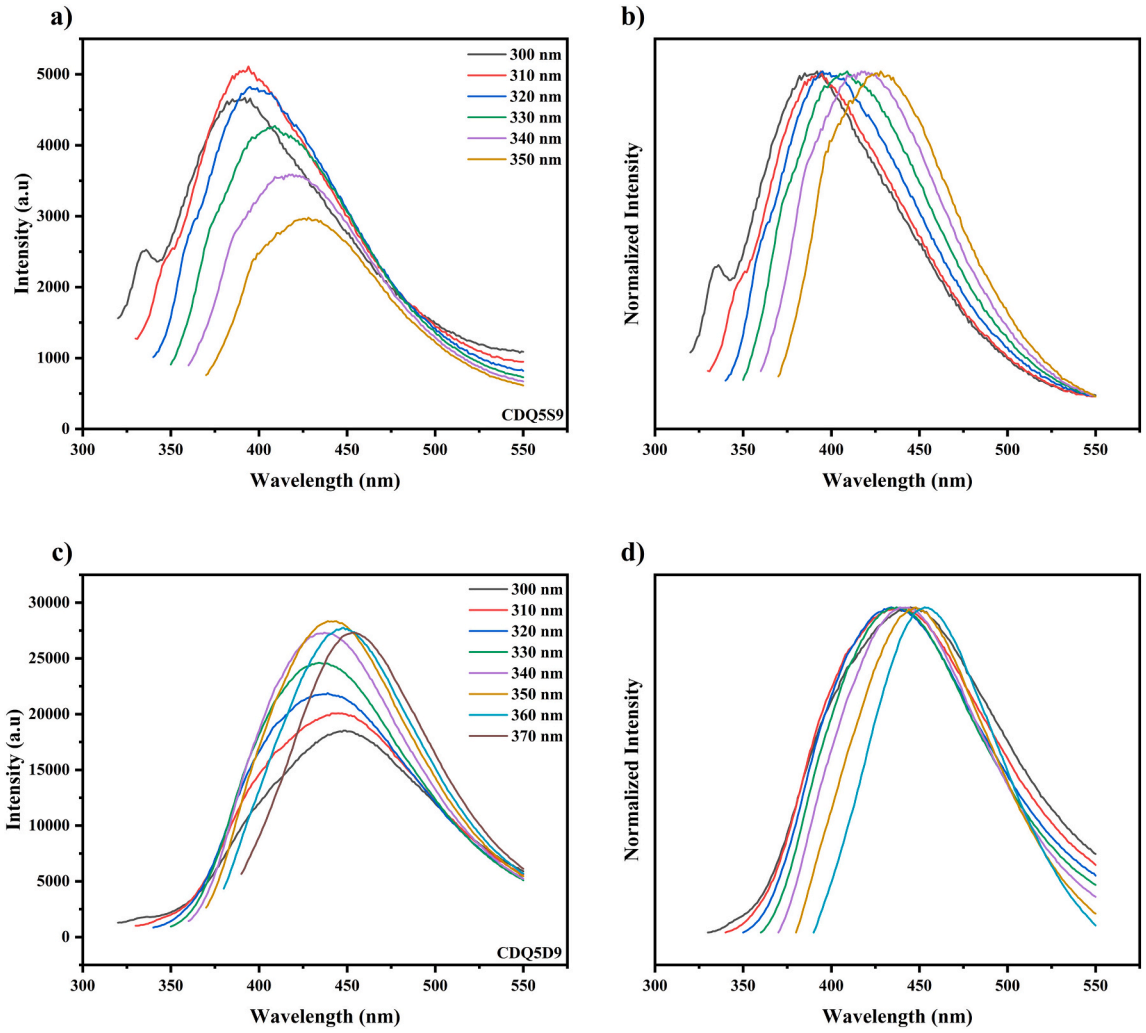

Fig. 6. Fluorescence spectroscopy and normalized fluorescence intensity of (a) CDQ5S9 and (c) CDQ5D9 samples.

properties to the surface state and functional groups inserted by incorporating the doping agent [62]. Furthermore, the emission wavelengths for doped samples (Fig. 6c) shifted to higher values in contrast with non-doped ones (Fig. 6a). We could explain this displacement behavior by the broad distribution of different emissive sites in the doped CDs, in accordance with the report by Sun et al. [63].

The non-doped sample, CDQ5S9, reached the maximum fluorescence intensity at 310 nm, and the observed emission was 394 nm. The doped sample, CDQ5D9, achieved the intensity maximum at the 350 nm excitation, and the observed emission shifted to the 444 nm range. Excitation after the UV region on the chitosan-based carbon dots resulted in the diminishing of fluorescent intensity. Bao et al. synthesized CDs of several sizes, and they related that the emission peak shift was related to the decrease in carbon dot size [64]. Luo et al. stated that CDs with emissions at longer wavelengths could internalize into tissues and cells more effectively with brighter fluorescence emission in the red/near-IR regions [23,38].

3.3. Fungal cells fluorescence images

The bioimaging capability evaluation of the chitosan-based CDs was performed by employing confocal laser microscopy (Fig. 7). In the samples without CDs, there is no clear fluorescence emission of the *Candida albicans* cell culture when excited at the three analyzed wavelengths (Fig. 7a-c). On the other hand, after a brief incubation period (one hour), the cell culture with CDs presented bright fluorescence emission in three different excitation wavelengths, namely blue (405 nm), green (488 nm), and red (561) ranges (Fig. 7d-f).

The images suggest that chitosan-based CDs easily enter into the cells, probably through passive diffusion, accumulating in the cytoplasm until they reach their maximum concentration in a brief time, 30 min [65–67]. The high distribution observed in the cell membrane and the cytoplasm implies that they can be a propitious candidate for bioimaging applications. Furthermore, chitosan-based carbon quantum dots showed no cytotoxic effects on keratinocyte (HaCat) cultures in the absence of an external metabolizing source (S9 fraction) in the MTT assay, even at high concentrations (40 μg/ml). The MTT assay proved that the chitosan-based carbon dots at the concentration used for bioimaging purposes show no cytotoxicity.

Other biomarkers have been used in studies of Candida cells. Peptides conjugated with fluorescein isothiocyanate (FITC) to confocal laser scanner microscope (CLSM) analysis and flow cytometry [68,69]. Confocal laser scanning microscopy (CLSM) studies were conducted to examine the viability of the Candida cells stained with Syto 9, a green-fluorescent nuclear and chromosome that penetrates viable cells [70]. However, the emission range of Syto 9 and fluorescein isothiocyanate is in the green region of the spectrum. On the other hand, the chitosan-based carbon dots showed red, green, and blue emissions. This carbon dots' capability expands the possibilities of using carbon dots as a cell bioimaging agent.

Bhamore and coworkers reported the endocytosis of CDs by the fungal cell membrane of *Aspergillus aculeatus* and *Fomitopsis sp* [65]. The

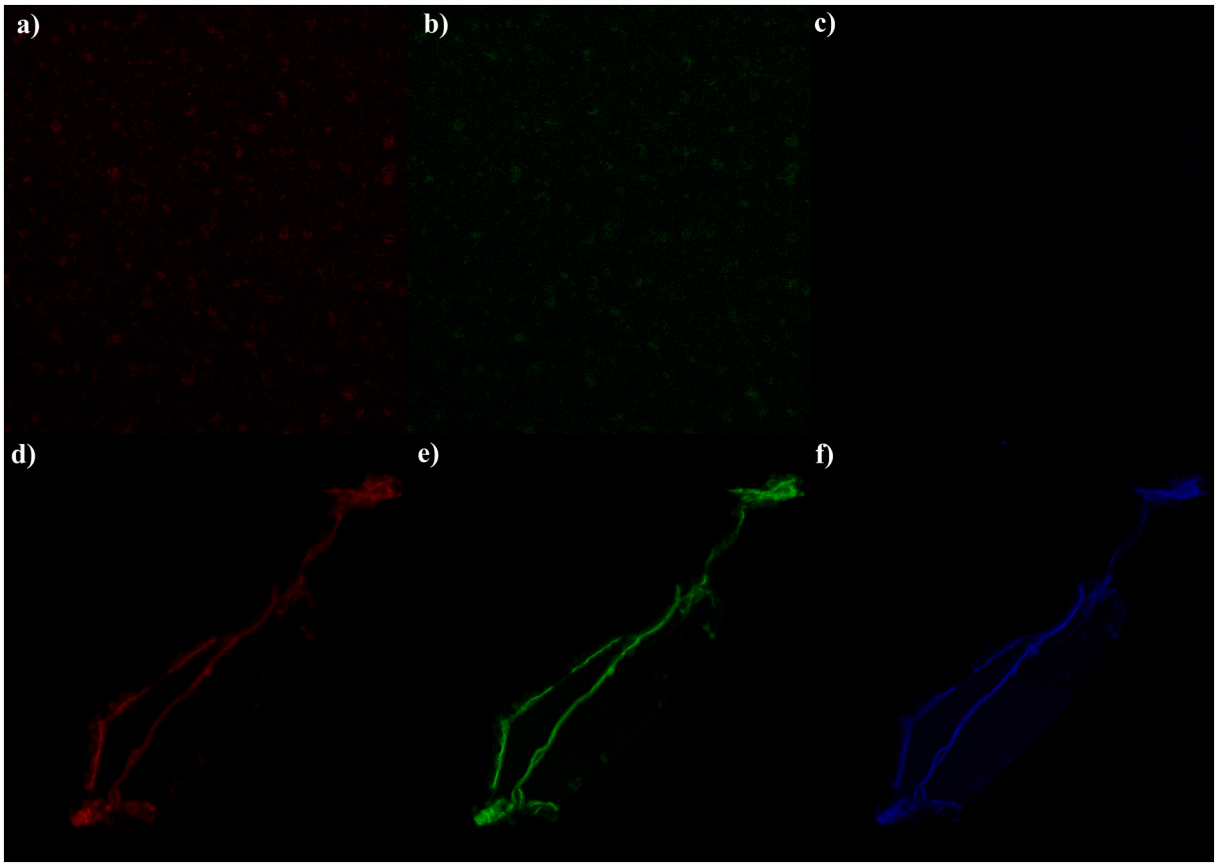

Fig. 7. Confocal microscope images. (a-c) *Candida albicans* cell culture excited at 405, 488, and 561 nm, respectively. (d-f) *Candida albicans* cell culture incubated with chitosan-based CDs excited in 405, 488, and 561 nm.

CDs are in the cell membrane and cytoplasm. Other cellular models were used to evaluate the CDs capability for bioimaging applications. Wey and coworkers used CDs for *in vivo* bioimaging of Zebrafish [71], Li et al. employed CDs as bioimaging probes for Hela cells [72], and Yan et al. applied CDs as a fluorescent reagent for biological imaging of bacteria that presented blue emission [73]. In all these reports, CDs are internalized in different cellular models, confirming their good capability as bioimaging agents.

In the work of Yu *et.al,* carbon dots were used for the fluorescent detection of *Candida albicans* [74]. Effective binding with *Candida albicans* cells was possible with the use of the antifungal drug amphotericin B. The binding between amphotericin B and *Candida albicans* cells occurs by hydrogen bonds between the carbonyl portion of the antifungal and the fungal cell membrane [75].

In our work, the chitosan-based carbon dots showed strong C═O stretching in the 1600 cm^{-1} region. The high content of carbonyl, hydroxyl and amino groups allows the chitosan-based carbon dots to bind to the ergosterol of the *Candida albicans* cell membrane [76]. Through hydrogen bonds, the carbonyl groups could open pores in the cell membrane allowing the chitosan-carbon dots to internalize and act as bioimaging agents.

4. Conclusion

We synthesized doped and non-doped chitosan-based CDs by one-step microwave synthesis and evaluated the influence of synthesis parameters on the CDs quantum yield. The association of factors molar ratio acetic acid/chitosan and the synergy of the doping agent and synthesis time was statistically more significant than individual parameters to obtain CDs with higher quantum yield. Our findings show that the 22:1 molar ratio with a synthesis time of 9.5 min showed the best quantum yield without the presence of the doping agent. In other words, it is statistically more favorable to combine the shorter synthesis time (9,5 min) and higher molar ratio (22:1) to obtain better quantum yields compared to the influence of the doping agent. More importantly, the chitosan-based carbon dots were able to specifically interact with the ergosterol of the *Candida albicans* cell membrane. This interaction allowed the carbon dots to internalize into the cytoplasm of the fungal cells. The chitosan-based carbon dots exhibited multicolor emission, corroborating their ability as a bioimaging agent.

CRediT authorship contribution statement

Bruno P. Oliveira: Conceptualization, preparation, Data curation, Investigation, Methodology, Writing-Original draft. **Nathalia U. C. Bessa:** Investigation. **Joice F. Nascimento:** Investigation. **Carolina S. P. Cavalcante:** Resources**,** Investigation, Writing-Original Draft. **Raquel O. S. Fontenelle:** Resources, Writing-Original Draft. **Flávia O. M. S. Abreu:** Conceptualization, Supervision, Formal analysis Writing-Reviewing and Editing; Project administration.

Declaration of competing interest

The authors declare that they have no known competing financial interests or personal relationships that could have appeared to influence the work reported in this paper.

Data availability

Data will be made available on request.

Acknowledgements

The authors would like to thank the Cearense Foundation of Scientific and Technological Support (FUNCAP), the National Council for Scientific and Technological Development (CNPq), and the State University of Ceara (UECE) Brazil for the granted scholarships. The authors also would like to thank the Central Analytical-UFC (funded by Finep-CT-INFRA, CAPES-Pró-Equipamentos, and MCTI-CNPq-SisNano2.0) for microscope confocal images, Chemistry Department Central Analytical for the fluorescence spectroscopy, Chemistry Institute Central Analytical for elemental analysis, Materials Engineering Department (UFRN) for atomic force microscopy measurements, and the Brazilian Agricultural Research Corporation (EMBRAPA) for Zeta Potential measurements.

Appendix A. Supplementary data

Supplementary data to this article can be found online at https://doi.org/10.1016/j.ijbiomac.2022.12.202.

References

[1] X. Xu, R. Ray, Y. Gu, H.J. Ploehn, L. Gearheart, K. Raker, W.A. Scrivens, Electrophoretic analysis and purification of fluorescent single-walled carbon nanotube fragments, J. Am. Chem. Soc. 126 (2004) 12736–12737, https://doi.org/10.1021/ja040082h.
[2] S.Y. Lim, W. Shen, Z. Gao, Carbon quantum dots and their applications, Chem. Soc. Rev. 44 (2015) 362–381, https://doi.org/10.1039/c4cs00269e.
[3] L. Li, X. Zheng, Y. Huang, L. Zhang, K. Cui, Y. Zhang, J. Yu, Addressable TiO2 nanotubes functionalized paper-based cyto-sensor with photocontrollable switch for highly-efficient evaluating surface protein expressions of cancer cells, Anal. Chem. 90 (2018) 13882–13890, https://doi.org/10.1021/acs.analchem.8b02849.
[4] P. Gong, L. Sun, F. Wang, X. Liu, Z. Yan, M. Wang, L. Zhang, Z. Tian, Z. Liu, J. You, Highly fluorescent N-doped carbon dots with two-photon emission for ultrasensitive detection of tumor marker and visual monitor anticancer drug loading and delivery, Chem. Eng. J. 356 (2019) 994–1002, https://doi.org/10.1016/j.cej.2018.09.100.
[5] Y. Wang, A. Hu, Carbon quantum dots: synthesis, properties and applications, J. Mater. Chem. C Mater. 2 (2014) 6921, https://doi.org/10.1039/C4TC00988F.
[6] X. Zhang, M. Jiang, N. Niu, Z. Chen, S. Li, S. Liu, J. Li, Natural-product-derived carbon dots: from natural products to functional materials, ChemSusChem. 11 (2018) 11–24, https://doi.org/10.1002/cssc.201701847.
[7] X. Wang, Y. Feng, P. Dong, J. Huang, A mini review on carbon quantum dots: preparation,properties, and electrocatalytic application, Front. Chem. 7 (2019) 1–9, https://doi.org/10.3389/fchem.2019.00671.
[8] T.v.de Medeiros, J. Manioudakis, F. Noun, J.R. Macairan, F. Victoria, R. Naccache, Microwave-assisted synthesis of carbon dots and their applications, J. Mater. Chem. C Mater. 7 (2019) 7175–7195, https://doi.org/10.1039/c9tc01640f.
[9] J. Sun, W. Wang, Q. Yue, Review on microwave-matter interaction fundamentals and efficient microwave-associated heating strategies, Materials 9 (2016), https://doi.org/10.3390/ma9040231.
[10] Y. Liu, N. Xiao, N. Gong, H. Wang, X. Shi, W. Gu, L. Ye, One-step microwave-assisted polyol synthesis of green luminescent carbon dots as optical nanoprobes, Carbon N. Y. 68 (2014) 258–264, https://doi.org/10.1016/j.carbon.2013.10.086.
[11] J. Zhou, H. Zhou, J. Tang, S. Deng, F. Yan, W. Li, M. Qu, Carbon dots doped with heteroatoms for fluorescent bioimaging: a review, Microchim. Acta 184 (2017) 343–368, https://doi.org/10.1007/s00604-016-2043-9.
[12] B.N. Jusuf, N.S. Sambudi, I. Isnaeni, S. Samsuri, Microwave-assisted synthesis of carbon dots from eggshell membrane ashes by using sodium hydroxide and their usage for degradation of methylene blue, J. Environ. Chem. Eng. 6 (2018) 7426–7433, https://doi.org/10.1016/j.jece.2018.10.032.
[13] J. Manioudakis, F. Victoria, C.A. Thompson, L. Brown, M. Movsum, R. Lucifero, R. Naccache, Effects of nitrogen-doping on the photophysical properties of carbon dots, J.Mater. Chem. C Mater. 7 (2019) 853–862, https://doi.org/10.1039/c8tc04821e.
[14] Z. Xu, C. Wang, K. Jiang, H. Lin, Y. Huang, C. Zhang, Microwave-assisted rapid synthesis of amphibious yellow fluorescent carbon dots as a colorimetric nanosensor for Cr(VI), Part. Part. Syst. Charact. 32 (2015) 1058–1062, https://doi.org/10.1002/ppsc.201500172.
[15] Ł. Janus, M. Piątkowski, J. Radwan-Pragłowska, D. Bogdał, D. Matysek, Chitosan-based carbon quantum dots for biomedical applications: synthesis and characterization, Nanomaterials 9 (2019) 274, https://doi.org/10.3390/nano9020274.
[16] Y. Jiang, J. Wu, Recent development in chitosan nanocomposites for surface-based biosensor applications, Electrophoresis 40 (2019) 2084–2097, https://doi.org/10.1002/elps.201900066.
[17] M. Maruthapandi, K. Sharma, J.H.T. Luong, A. Gedanken, Antibacterial activities of microwave-assisted synthesized polypyrrole/chitosan and poly (pyrrole-N-(1-naphthyl) ethylenediamine) stimulated by C-dots, Carbohydr. Polym. 243 (2020), 116474, https://doi.org/10.1016/j.carbpol.2020.116474.
[18] J. Zhan, R. Peng, S. Wei, J. Chen, X. Peng, B. Xiao, Ethanol-precipitation-assisted highly efficient synthesis of nitrogen-doped carbon quantum dots from chitosan, ACS Omega 4 (2019) 22574–22580, https://doi.org/10.1021/acsomega.9b03318.
[19] J. Song, L. Zhao, Y. Wang, Y. Xue, Y. Deng, X. Zhao, Q. Li, Carbon quantum dots prepared with chitosan for synthesis of CQDS/auNPs for iodine ions detection, Nanomaterials 8 (2018) 1043, https://doi.org/10.3390/NANO8121043.
[20] X. Liu, J. Pang, F. Xu, X. Zhang, Simple approach to synthesize amino-functionalized carbon dots by carbonization of chitosan, Sci. Rep. 6 (2016) 1–8, https://doi.org/10.1038/srep31100.
[21] A. Ray Chowdhuri, S. Tripathy, C. Haldar, S. Roy, S.K. Sahu, Single step synthesis of carbon dot embedded chitosan nanoparticles for cell imaging and hydrophobic drug delivery, J. Mater. Chem. B 3 (2015) 9122–9131, https://doi.org/10.1039/C5TB01831E.
[22] Y. Zhou, T. Wu, L. Duan, G. Hu, J. Shi, Y. Nie, Y. Zhou, Synthesizing carbon dots with functional preservation strategy as a facile ratiometric fluorescent sensing platform for monitoring hypochlorite in living cells and zebrafish, Sensors Actuators B Chem. 365 (2022), https://doi.org/10.1016/j.snb.2022.131946.
[23] P.G. Luo, S. Sahu, S.T. Yang, S.K. Sonkar, J. Wang, H. Wang, G.E. Lecroy, L. Cao, Y. P. Sun, Carbon "quantum" dots for optical bioimaging, J. Mater. Chem. B 1 (2013) 2116–2127, https://doi.org/10.1039/c3tb00018d.
[24] S.T. Yang, L. Cao, P.G. Luo, F. Lu, X. Wang, H. Wang, M.J. Meziani, Y. Liu, G. Qi, Y. P. Sun, Carbon dots for optical imaging in vivo, J. Am. Chem. Soc. 131 (2009) 11308–11309, https://doi.org/10.1021/ja904843x.
[25] H. Liu, J. Ding, K. Zhang, L. Ding, Construction of biomass carbon dots based fluorescence sensors and their applications in chemical and biological analysis, TrAC Trends Anal. Chem. 118 (2019) 315–337, https://doi.org/10.1016/j.trac.2019.05.051.
[26] N. Tejwan, S.K. Saha, J. Das, Multifaceted applications of green carbon dots synthesized from renewable sources, Adv. Colloid InterfaceSci. 275 (2020), 102046, https://doi.org/10.1016/j.cis.2019.102046.
[27] X. Gong, W. Lu, M.C. Paau, Q. Hu, X. Wu, S. Shuang, C. Dong, M.M.F. Choi, Facile synthesis of nitrogen-doped carbon dots for Fe3+ sensing and cellular imaging, Anal. Chim. Acta 861 (2015) 74–84, https://doi.org/10.1016/j.aca.2014.12.045.
[28] R. Atchudan, T.N.J.I. Edison, D. Chakradhar, S. Perumal, J.J. Shim, Y.R. Lee, Facile green synthesis of nitrogen-doped carbon dots using Chionanthus retusus fruit extract and investigation of their suitability for metal ion sensing and biological applications, Sensor Actuators B Chem. 246 (2017) 497–509, https://doi.org/10.1016/j.snb.2017.02.119.
[29] J.R. Lakowicz, Principles of Fluorescence Spectroscopy, Third edit, 2006. Sp.
[30] T. Mosmann, Rapid colorimetric assay for cellular growth and survival: application to proliferation and cytotoxicity assays, <sb:contribution><sb:title>J. Immunol. </sb:title></sb:contribution><sb:host><sb:issue><sb:series><sb:title>Methods</sb:title></sb:series></sb:issue></sb:host> 65 (1983) 55–63.
[31] Y. Wang, J. Zheng, J. Wang, Y. Yang, X. Liu, Rapid microwave-assisted synthesis of highly luminescent nitrogen-doped carbon dots for white light-emitting diodes, Opt. Mater. 73 (2017) 319–329, https://doi.org/10.1016/j.optmat.2017.08.032.
[32] J. Briscoe, A. Marinovic, M. Sevilla, S. Dunn, M. Titirici, Biomass-derived carbon quantum dot sensitizers for solid-state nanostructured solar cells, Angew.Chem.Int. Ed. 54 (2015) 4463–4468, https://doi.org/10.1002/anie.201409290.
[33] C.P. Pinheiro, T.G. Mello, M.L.G. Vieira, L.A.A. Pinto, Chitosan-coated different particles in spouted bed and their use in dye continuous adsorption system, Environ. Sci. Pollut. Res. 26 (2019) 28510–28523, https://doi.org/10.1007/s11356-019-04905-9.
[34] G.L. Dotto, R. Ocampo-Pérez, J.M. Moura, T.R.S. Cadaval, L.A.A. Pinto, Adsorption rate of Reactive Black 5 on chitosan based materials: geometry and swelling effects, Adsorption 22 (2016) 973–983, https://doi.org/10.1007/s10450-016-9804-y.
[35] J.R. Bhamore, S. Jha, T.J. Park, S.K. Kailasa, Fluorescence sensing of Cu2+ ion and imaging of fungal cell by ultra-small fluorescent carbon dots derived from Acacia concinna seeds, Sensors Actuators B Chem. 277 (2018) 47–54, https://doi.org/10.1016/j.snb.2018.08.149.
[36] Y. Shi, X. Liu, M. Wang, J. Huang, X. Jiang, J. Pang, F. Xu, X. Zhang, Synthesis of N-doped carbon quantum dots from bio-waste lignin for selective irons detection and cellular imaging, Int. J. Biol. Macromol. 128 (2019) 537–545, https://doi.org/10.1016/j.ijbiomac.2019.01.146.
[37] M.L. Liu, B. bin Chen, C.M. Li, C.Z. Huang, Carbon dots: synthesis, formation mechanism, fluorescence origin and sensing applications, Green Chem. 21 (2019) 449–471, https://doi.org/10.1039/C8GC02736F.
[38] B. Wang, H. Cai, G.I.N. Waterhouse, X. Qu, B. Yang, S. Lu, Carbon dots in bioimaging, biosensing and therapeutics: a comprehensive review, SmallSci. 2 (2022), 2200012, https://doi.org/10.1002/smsc.202200012.
[39] K. Hola, Y. Zhang, Y. Wang, E.P. Giannelis, R. Zboril, A.L. Rogach, Carbon dots - emerging light emitters for bioimaging, cancer therapy and optoelectronics, Nano Today 9 (2014) 590–603, https://doi.org/10.1016/j.nantod.2014.09.004.
[40] H. Li, X. He, Z. Kang, H. Huang, Y. Liu, J. Liu, S. Lian, C.H.A. Tsang, X. Yang, S. T. Lee, Water-soluble fluorescent carbon quantum dots and photocatalyst design, Angew.Chem.Int.Ed. 49 (2010) 4430–4434, https://doi.org/10.1002/anie.200906154.
[41] M.R. Lima, H.C.B. Paula, F.O.M.S. Abreu, R.B.C. da Silva, F.M. Sombra, R.C.M. de Paula, Hydrophobization of cashew gum by acetylation mechanism and amphotericin B encapsulation, Int. J. Biol. Macromol. 108 (2018) 523–530, https://doi.org/10.1016/j.ijbiomac.2017.12.047.
[42] X. Gong, M. Chin Paau, Q. Hu, S. Shuang, C. Dong, M.M.F. Choi, UHPLC combined with mass spectrometric study of as-synthesized carbon dots samples, Talanta 146 (2016) 340–350, https://doi.org/10.1016/j.talanta.2015.08.051.
[43] A. Pal, K. Ahmad, D. Dutta, A. Chattopadhyay, Boron doped carbon dots with unusually high photoluminescence quantum yield for ratiometric intracellular pH

sensing, ChemPhysChem 20 (2019) 1018–1027, https://doi.org/10.1002/cphc.201900140.
[44] D.W. Zhang, N. Papaioannou, N.M. David, H. Luo, H. Gao, L.C. Tanase, T. Degousée, P. Samorì, A. Sapelkin, O. Fenwick, M.M. Titirici, S. Krause, Photoelectrochemical response of carbon dots (CDs) derived from chitosan and their use in electrochemical imaging, Mater. Horiz. 5 (2018) 423–428, https://doi.org/10.1039/c7mh00784a.
[45] D. Chowdhury, N. Gogoi, G. Majumdar, Fluorescent carbon dots obtained from chitosan gel, RSC Adv. 2 (2012) 12156–12159, https://doi.org/10.1039/c2ra21705h.
[46] Z. Shekarbeygi, N. Farhadian, M. Ansari, M. Shahlaei, S. Moradi, An innovative green sensing strategy based on Cu-doped Tragacanth/Chitosan nano carbon dots for isoniazid detection, Spectrochim. Acta A Mol. Biomol. Spectrosc. 228 (2020), 117848, https://doi.org/10.1016/j.saa.2019.117848.
[47] S. Mitra, S. Chandra, T. Kundu, R. Banerjee, P. Pramanik, A. Goswami, Rapid microwave synthesis of fluorescent hydrophobic carbon dots, RSC Adv. 2 (2012) 12129–12131, https://doi.org/10.1039/c2ra21048g.
[48] O. Lv, Y. Tao, Y. Qin, C. Chen, Y. Pan, L. Deng, L. Liu, Y. Kong, Highly fluorescent and morphology-controllable graphene quantum dots-chitosan hybrid xerogels for in vivo imaging and pH-sensitive drug carrier, Mater. Sci. Eng. C 67 (2016) 478–485, https://doi.org/10.1016/j.msec.2016.05.031.
[49] F.O.M. da Silva Abreu, B.P. de Oliveira, Ultra-small carbon dots for sensing and imaging of chemical species, in: C.M.H. Suresh Kumar Kailasa (Ed.), Carbon Dots in Analytical Chemistry, 1st ed., Elsevier, Amsterdam, 2023, pp. 255–270, https://doi.org/10.1016/B978-0-323-98350-1.00003-7.
[50] Z. Jiang, A. Nolan, J.G.A. Walton, A. Lilienkampf, R. Zhang, M. Bradley, Photoluminescent carbon dots from 1,4-addition polymers, Chem. Eur. J. 20 (2014) 10926–10931, https://doi.org/10.1002/chem.201403076.
[51] L. Zhao, Y. Wang, X. Zhao, Y. Deng, Y. Xia, Facile synthesis of nitrogen-doped carbon quantum dots with chitosan for fluorescent detection of Fe3+, Polymers (Basel) 11 (2019) 1–12, https://doi.org/10.3390/polym11111731.
[52] H. Li, F.Q. Shao, S.Y. Zou, Q.J. Yang, H. Huang, J.J. Feng, A.J. Wang, Microwave-assisted synthesis of N, P-doped carbon dots for fluorescent cell imaging, Microchim. Acta 183 (2016) 821–826, https://doi.org/10.1007/s00604-015-1714-2.
[53] X. Gong, Q. Zhang, Y. Gao, S. Shuang, M.M.F. Choi, C. Dong, Phosphorus and nitrogen dual-doped hollow carbon dot as a nanocarrier for doxorubicin delivery and biological imaging, ACS Appl. Mater. Interfaces 8 (2016) 11288–11297, https://doi.org/10.1021/acsami.6b01577.
[54] A. Bhati, S.R. Anand, D. Saini, S.K.Sonkar Gunture, Sunlight-induced photoreduction of Cr(VI) to Cr(III) in wastewater by nitrogen-phosphorus-doped carbon dots, NPJ CleanWater 2 (2019) 1–9, https://doi.org/10.1038/s41545-019-0036-z.
[55] Y.M. Bakier, M. Ghali, A. Elkun, A.M. Beltagi, W.K. Zahra, Static interaction between colloidal carbon nano-dots and aniline: a novel platform for ultrasensitive detection of aniline in aqueous medium, Mater. Res. Bull. 134 (2021), 111119, https://doi.org/10.1016/j.materresbull.2020.111119.
[56] S. Sahu, B. Behera, T.K. Maiti, S. Mohapatra, Simple one-step synthesis of highly luminescent carbon dots from orange juice: application as excellent bio-imaging agents, Chem. Commun. 48 (2012) 8835–8837, https://doi.org/10.1039/c2cc33796g.
[57] H. Ding, S.B. Yu, J.S. Wei, H.M. Xiong, Full-color light-emitting carbon dots with a surface-state-controlled luminescence mechanism, ACS Nano 10 (2016) 484–491, https://doi.org/10.1021/acsnano.5b05406.
[58] P. Anilkumar, X. Wang, L. Cao, S. Sahu, J.-H. Liu, P. Wang, K. Korch, K. N. Tackett II, A. Parenzan, Y.-P. Sun, Toward quantitatively fluorescent carbon-based "quantum" dots, Nanoscale 3 (2011) 2023, https://doi.org/10.1039/c0nr00962h.
[59] Y.P. Sun, X. Wang, F. Lu, L. Cao, M.J. Meziani, P.G. Luo, L. Gu, L. Monica Veca, Doped carbon nanoparticles as a new platform for highly photoluminescent dots, J. Phys. Chem. C 112 (2008) 18295–18298, https://doi.org/10.1021/jp8076485.
[60] Y. Dong, H. Pang, H.bin Yang, C. Guo, J. Shao, Y. Chi, C.M. Li, T. Yu, Carbon-based dots co-doped with nitrogen and sulfur for high quantum yield and excitation-independent emission, Angew. Chem. Int. Ed. 52 (2013) 7800–7804, https://doi.org/10.1002/anie.201301114.
[61] W. Lu, X. Gong, M. Nan, Y. Liu, S. Shuang, C. Dong, Comparative study for N and S doped carbon dots: synthesis, characterization and applications for Fe3+ probe and cellular imaging, Anal. Chim. Acta 898 (2015) 116–127, https://doi.org/10.1016/j.aca.2015.09.050.
[62] M.K. Barman, B. Jana, S. Bhattacharyya, A. Patra, Photophysical properties of doped carbon dots (N, P, and B) and their influence on electron/hole transfer in carbon dots-nickel (II) phthalocyanine conjugates, J. Phys. Chem. C 118 (2014) 20034–20041, https://doi.org/10.1021/jp507080c.
[63] Y.P. Sun, B. Zhou, Y. Lin, W. Wang, K.A.S. Fernando, P. Pathak, M.J. Meziani, B. A. Harruff, X. Wang, H. Wang, P.G. Luo, H. Yang, M.E. Kose, B. Chen, L.M. Veca, S. Y. Xie, Quantum-sized carbon dots for bright and colorful photoluminescence, J. Am. Chem. Soc. 128 (2006) 7756–7757, https://doi.org/10.1021/ja062677d.
[64] L. Bao, Z.L. Zhang, Z.Q. Tian, L. Zhang, C. Liu, Y. Lin, B. Qi, D.W. Pang, Electrochemical tuning of luminescent carbon nanodots: from preparation to luminescence mechanism, Adv. Mater. 23 (2011) 5801–5806, https://doi.org/10.1002/adma.201102866.
[65] J.R. Bhamore, S. Jha, T.J. Park, S.K. Kailasa, T. Jung, S. Kumar, T.J. Park, S. K. Kailasa, Green synthesis of multi-color emissive carbon dots from Manilkara zapota fruits for bioimaging of bacterial and fungal cells, J. Photochem. Photobiol. B 191 (2019) 150–155, https://doi.org/10.1016/j.jphotobiol.2018.12.023.
[66] A. Loukanov, R. Sekiya, M. Yoshikawa, N. Kobayashi, Y. Moriyasu, S. Nakabayashi, Photosensitizer-conjugated ultrasmall carbon nanodots as multifunctional fluorescent probes for bioimaging, J. Phys. Chem. C 120 (2016) 15867–15874, https://doi.org/10.1021/acs.jpcc.5b11721.
[67] P.K. Pandey, K. Preeti, T. Rawat, H.B. Prasad, Bohidar, multifunctional, fluorescent DNA-derived carbon dots for biomedical applications: bioimaging, luminescent DNA hydrogels, and dopamine detection, J. Mater. Chem. B 8 (2020) 1277–1289, https://doi.org/10.1039/c9tb01863h.
[68] E. Galdiero, E. de Alteriis, A. de Natale, A. D'Alterio, A. Siciliano, M. Guida, L. Lombardi, A. Falanga, S. Galdiero, Eradication of Candida albicans persister cell biofilm by the membranotropic peptide gH625, Sci. Rep. 10 (2020), https://doi.org/10.1038/s41598-020-62746-w.
[69] C.S.P. Cavalcante, F.L.L. de Aguiar, R.O.S. Fontenelle, R.R.de P.P.B.de Menezes, A. M.C. Martins, C.B. Falcão, D. Andreu, G. Rádis-Baptista, Insights into the candidacidal mechanism of Ctn[15-34] - A carboxyl-terminal, crotalicidin-derived peptide related to cathelicidins, J. Med. Microbiol. 67 (2018) 129–138, https://doi.org/10.1099/jmm.0.000652.
[70] F.L.L. de Aguiar, N.C. Santos, C.S.de P. Cavalcante, D. Andreu, G.R. Baptista, S. Gonçalves, Antibiofilm activity on candida albicans and mechanism of action on biomembrane models of the antimicrobial peptide Ctn[15–34], Int. J. Mol. Sci. 21 (2020) 1–15, https://doi.org/10.3390/ijms21218339.
[71] X. Wei, L. Li, J. Liu, L. Yu, H. Li, F. Cheng, X. Yi, J. He, B. Li, Green synthesis of fluorescent carbon dots from gynostemma for bioimaging and antioxidant in zebrafish, ACS Appl. Mater. Interfaces 11 (2019) 9832–9840, https://doi.org/10.1021/acsami.9b00074.
[72] H. Li, F.Q. Shao, H. Huang, J.J. Feng, A.J. Wang, Eco-friendly and rapid microwave synthesis of green fluorescent graphitic carbon nitride quantum dots for vitro bioimaging, Sensors Actuators B Chem. 226 (2016) 506–511, https://doi.org/10.1016/j.snb.2015.12.018.
[73] D. Shi, F. Yan, T. Zheng, Y. Wang, X. Zhou, L. Chen, P-doped carbon dots act as a nanosensor for trace 2,4,6-trinitrophenol detection and a fluorescent reagent for biological imaging, RSC Adv. 5 (2015) 98492–98499, https://doi.org/10.1039/c5ra18800h.
[74] D. Yu, L. Wang, H. Zhou, X. Zhang, L. Wang, N. Qiao, Fluorimetric detection of Candida albicans using cornstalk N-carbon quantum dots modified with amphotericin B, Bioconjug. Chem. 30 (2019) 966–973, https://doi.org/10.1021/acs.bioconjchem.9b00131.
[75] B. Chudzik, M. Koselski, A. Czuryło, K. Trębacz, M. Gagoś, A new look at the antibiotic amphotericin B effect on Candida albicans plasma membrane permeability and cell viability functions, Eur. Biophys. J. 44 (2015) 77–90, https://doi.org/10.1007/s00249-014-1003-8.
[76] R. Laniado-Laborín, M.N. Cabrales-Vargas, Amphotericin B: side effects and toxicity, Rev. Iberoam. Micol. 26 (2009) 223–227, https://doi.org/10.1016/j.riam.2009.06.003.